

# Effect of Electrolyte pH and Deposition Time on the Microstructure and Magnetic Properties of Electrodeposited Fe<sub>2</sub>CoSn Heusler Alloy

Shengjie Gao, Yicai Liu, Xinli Kou \*

Key Laboratory for Magnetism and Magnetic Materials of the Ministry of Education, School of Physical Science and Technology, Lanzhou University, Lanzhou 730000, China

\*E-mail: [kouxl@lzu.edu.cn](mailto:kouxl@lzu.edu.cn)

Received: 14 July 2015 / Accepted: 17 August 2015 / Published: 26 August 2015

---

Electrochemical synthesis of Fe<sub>2</sub>CoSn Heusler alloy is reported in the present study. The effects of electrolyte pH and deposition time on the morphology, structure, chemical composition, and magnetic properties of the deposited films were investigated. The microstructure dependence of magnetic properties of the samples was discussed. It was found that the Fe<sub>2</sub>CoSn Heusler alloy with nominal 2: 1: 1 composition can be obtained when the pH is 7.0 and the deposition time is 15 min. The electrodeposited Fe<sub>2</sub>CoSn film is composed of many fine particles with the size of about 20-30 nm. A homogeneous distribution of Fe, Co and Sn elements in the Fe<sub>2</sub>CoSn film was illustrated. Magnetic measurement indicates that the electrodeposited Fe<sub>2</sub>CoSn alloy is ferromagnetic at room temperature with the magnetic moment of about 3.5  $\mu_B$ /f.u and coercivity of 48 Oe. The results showed that the electrodeposited Fe<sub>2</sub>CoSn film is economical and suitable for technological applications.

---

**Keywords:** Fe<sub>2</sub>CoSn alloy; Electrodeposition; Microstructure; Magnetic properties

## 1. INTRODUCTION

The Heusler compounds, marked with the formula X<sub>2</sub>YZ (X and Y are transition metals and Z is a main group element), are used widely in today's electronics industry and various engineering applications [1]. Among them, the group of Fe<sub>2</sub>-based Heusler compounds exhibit very interesting structure, electronic and magnetic properties [2-4]. The Fe<sub>2</sub>-based Heusler compounds predicted to possess a large magnetization and high Curie temperature are of special interest for potential magnetic applications [5,6]. Up to now, a number of Fe<sub>2</sub>-based Heusler compounds have been synthesized and their crystal structures and properties have been investigated [7-9]. Fe<sub>2</sub>-based Heusler compounds have been prepared mostly by arc melting, molecular beam epitaxy and ball-milling method [8-11].

Recently, the electrochemical deposition method for the synthesis of compositionally modulated alloys has attracted great interest because electrodeposition is a simple and economic method without high temperature and high pressure [12-15]. By adjusting the deposition parameters such as the electrolyte concentration, pH, current density, et. al, it can be possible to control and optimize the structure, morphology and properties of electrodeposited films. In our previous work, Co<sub>2</sub>-based Heusler alloy have been synthesized by using the electrodeposition method [16]. The effects of the electrodeposition current density on microstructure and magnetic properties of the samples have been investigated in detail. The low-cost electrodeposition method is believed to have potential applications in synthesizing other Heusler alloys. However, up to now, there are no studies on the synthesis of Fe<sub>2</sub>-based Heusler alloys using the electrodeposition method. In the present work, the preparation of Fe<sub>2</sub>-based Heusler alloy by using the electrodeposition method will be studied.

The magnetism of Fe<sub>2</sub>-based Heusler alloys has been predicted by Gilleben et. al. using first-principle computation methods [17]. Among various Fe<sub>2</sub>-based Heusler alloys, the Fe<sub>2</sub>CoSn Heusler alloy has attracted our attention because it was predicted to have considerably large magnetic moment and cheap. It is noteworthy that the elements present in Fe<sub>2</sub>CoSn Heusler compounds, that is, Fe, Co and Sn, can be electrodeposited in aqueous solutions [18-20]. The standard redox potentials of Fe<sup>2+</sup>/Fe, Co<sup>2+</sup>/Co and Sn<sup>2+</sup>/Sn in aqueous solutions are -0.447 V, -0.28 V and -0.14 V [21], respectively. If using an appropriate complexing agent such as sodium gluconate (C<sub>6</sub>H<sub>11</sub>O<sub>7</sub>Na) to facilitate the bringing together of the electrode potentials of the Fe, Co and Sn, codeposition of iron, cobalt and tin to form a Fe<sub>2</sub>CoSn Heusler alloy is possible. Hence, this paper will focus on the electrochemical deposition of Fe<sub>2</sub>CoSn Heusler alloy. Specifically, the effects of the electrolyte pH and deposition time on structure, chemical composition, morphology and magnetic properties of the samples will be investigated in detail.

## 2. EXPERIMENTAL

The electrodepositions were performed in a two electrode system. The anode was a high density graphite sheet with a working surface area of 6 cm<sup>2</sup>. Copper cathodes (99.9% pure copper foil) were used with a working surface area of 2.0 cm<sup>2</sup>. Before deposition, the copper substrates were polished, degreased and rinsed with deionized water to ensure a cleaner and smoother surface for the following electrodeposition. Then, the cathodes were electropolished for 6 minutes at a current of 2 A in a solution comprised of 80% (v/v) phosphoric acid, 10% (v/v) methanol and 10% (v/v) deionized water. After that the cathodes were rinsed with deionized water and immediately transferred into the plating bath.

The plating cell used had a 50 mL capacity with 40 mL of electrolyte being used for each deposition study. The compositions of electrolytes and electrodeposition parameters were listed in Table 1. Saccharin, ascorbic acid and boric acid were used as brightener, stabilizer and buffering agent, respectively. NaCl was added in the electrolytes to promote the bath conductivity. PH value of the bath was adjusted by using additions of NaOH or H<sub>2</sub>SO<sub>4</sub>, respectively.

**Table 1.** Bath composition and electrodeposition parameters.

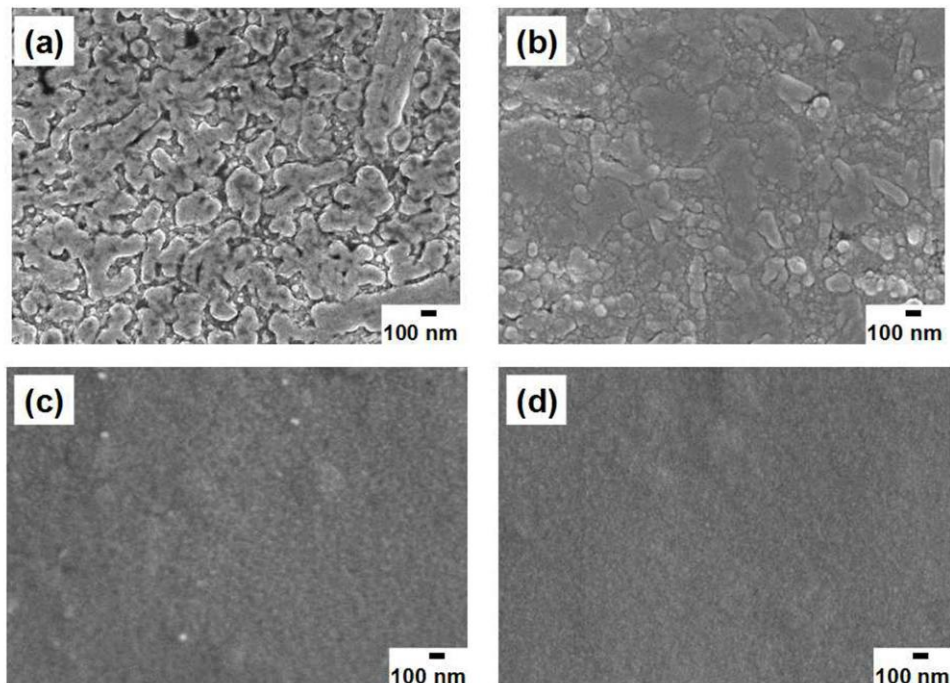
Bath composition	Concentration (g/L)	Electrodeposition parameter	Value
CoSO <sub>4</sub> ·7H <sub>2</sub> O	17.6	Current density	1.25 (A/dm <sup>2</sup> )
FeSO <sub>4</sub> ·7H <sub>2</sub> O	34.8	pH value	5.0, 6.0, 7.0, 8.0
SnSO <sub>4</sub>	2.2	Temperature	60 (°C)
Sodium gluconate	150	Deposition time	5-15 (min)
Peptone	0.1		
boric acid	23.0		
NaCl	22.0		
saccharin	2.5		
ascorbic acid	2.5		

The crystal structure of the samples was analyzed using X-ray diffraction (XRD) [Rigaku D/MAX-2400] with Cu  $K\alpha$  radiation ( $\lambda = 1.54056 \text{ \AA}$ ). The surface morphology and chemical composition of the deposited films were characterized by a JEOL JSM-6701F scanning electron microscope (SEM) operating at an accelerating voltage of 5.0 kV and an energy dispersion spectroscopy (EDS) operating at an accelerating voltage of 20.0 kV. The magnetic properties of the samples were measured by a Lake Shore 7304 vibrating sample magnetometer (VSM) at room temperature.

### 3. RESULTS AND DISCUSSION

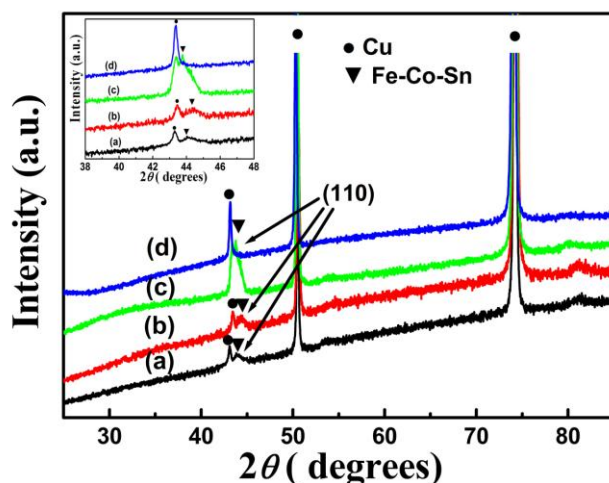
#### 3.1. Effects of pH value

Fig. 1 shows the surface morphologies of the samples deposited at different pH values. When the PH is 5.0 (Fig. 1a), the surface is composed of irregular particles and flakey agglomerates with the size of 100-800 nm. Some holes can be observed on the surface. When the PH is increased to 6.0 (Fig. 1b), the holes nearly disappear and the surface becomes more compacted. As the PH rises to 7.0 (Fig. 1c), the film is full of sphere-like particles with the size of about 20-30 nm. With further increase of the pH to 8.0 (Fig. 1d), the image shows fine particles of about 10 nm with a good coverage of the surface. It can be seen that the surface morphologies of our samples are strongly influenced by the electrolyte pH. The morphology of the samples can be explained by the hydrogen evolution occurred at the cathode surface. When the pH increases from 5.0 to 6.0, the surface of the films becomes less defective because of the weakening of hydrogen evolution at higher pH [22, 23]. As the pH value reaches up to 7.0-8.0, lower H<sup>+</sup> concentration depresses the evolution of hydrogen and less current is consumed on the hydrogen evolution leading to a higher current efficiency [23]. As a result, the deposition rate becomes larger, the concentration of the metal ions near the cathode surface decreases more than that in the electrolyte, then the concentration polarization takes place, the deposit changes to the fine powder [24, 25].



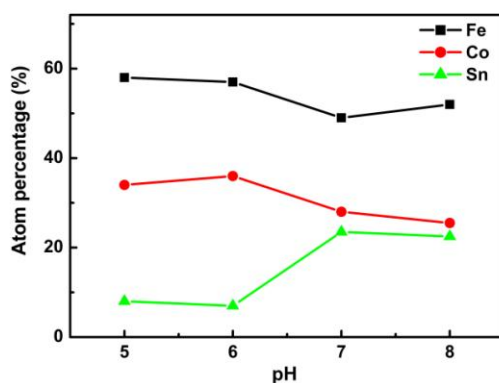
**Figure 1.** SEM images of the samples deposited at different pH values. (a) 5.0; (b) 6.0; (c) 7.0; (d) 8.0.

Fig. 2 shows the XRD patterns of the samples deposited at different pH values on a Cu substrate. In all the X-ray diffractograms, the diffraction peaks at about  $2\theta = 43.3^\circ$ ,  $50.4^\circ$  and  $74.1^\circ$  belong to the (111), (200) and (220) reflections of Cu substrate. It can be seen that when the pH value is 5.0-7.0 (Fig. 2a-c), besides the peaks from the Cu substrate, the diffraction peak at about  $2\theta = 44.0^\circ$  is present which corresponds to the (110) characteristic reflection of body-centered cubic (bcc) structure. The inset in Fig. 2 shows the magnified (110) diffraction peaks of the XRD patterns. When the PH value is 8.0 (Fig. 2d), only the diffraction peaks of Cu substrate are observed. The absence of Fe-Co-Sn diffraction peaks is probably due to the high deposition rate accelerate the nucleation and prevent the crystal growth [26].



**Figure 2.** XRD patterns of the samples deposited at different pH values. (a) 5.0; (b) 6.0; (c) 7.0; (d) 8.0. The inset shows the magnified (110) diffraction peaks of the XRD patterns.

The average elemental composition of the samples was determined by EDS and the dependences of Fe, Co and Sn content in the samples on pH value are shown in Fig. 3. It can be seen that as the pH values varying from 5.0 to 8.0, the content of Fe and Co has a tendency to decrease and the content of Sn has a tendency to increase. As anomalous codeposition has been reported mainly in codeposition of iron-group metals, Fe is preferentially deposited compared to Sn, even if Fe is the less noble metal [27, 28]. When the pH is increased from 5.0-8.0, the deposition rate increases, the consumption rate of  $Fe^{2+}$  near the cathode surface exceeds its supplement rate. As a result,  $Fe^{2+}$  concentration at the cathode surface decreases and the Fe content in the deposit decreases. Accordingly, the suppression of Sn deposition by ferrous hydroxide is weakened which leads to the increase content of Sn.



**Figure 3.** The dependences of Fe, Co and Sn content in the samples on pH value.

Fig. 4 shows the hysteresis loops of the samples electrodeposited at different pH values. It can be seen that all the samples are ferromagnetic at room temperature. The inset in Fig. 4 displays the variation of the coercivity ( $H_C$ ) with pH value.

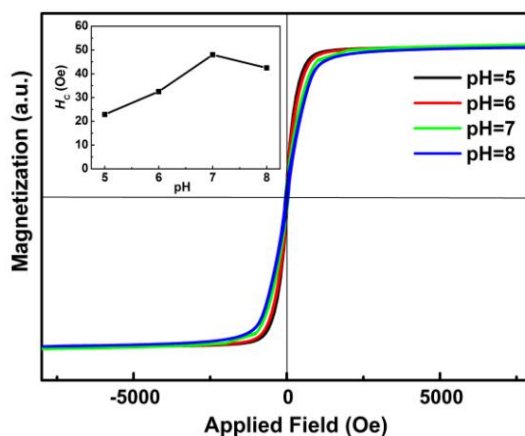


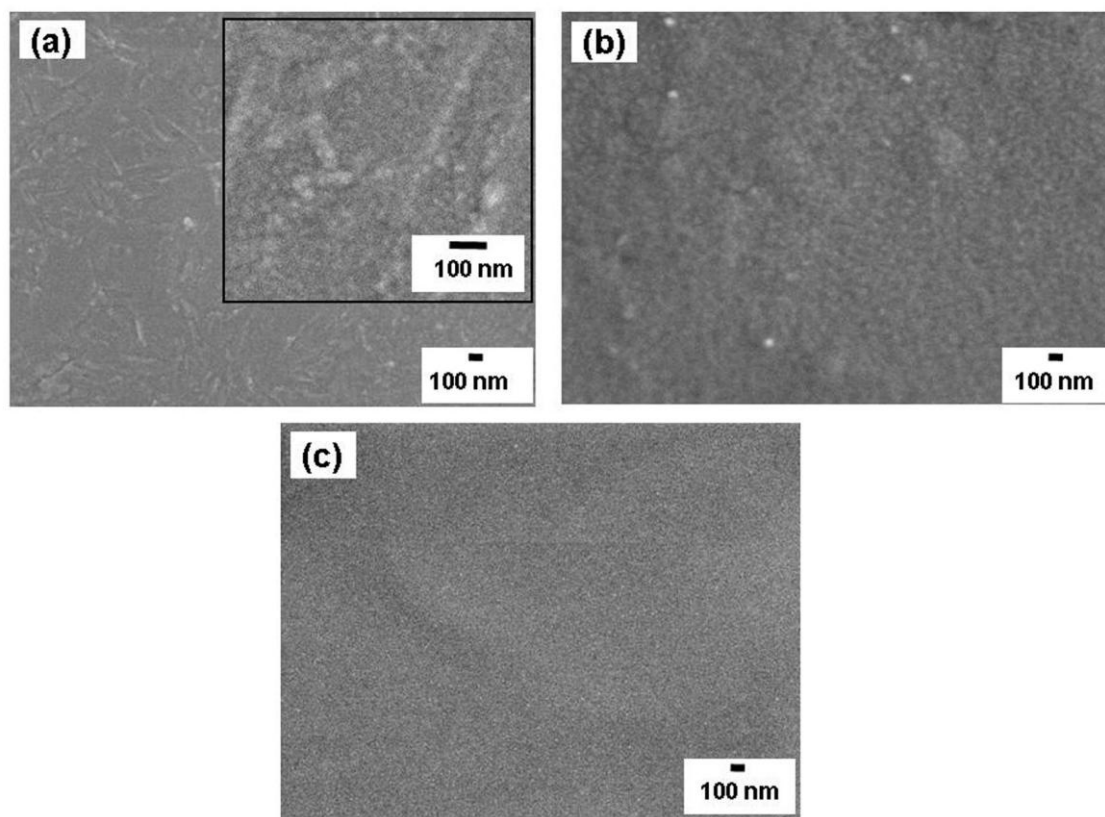
**Figure 4.** Hysteresis loops of the samples deposited at different pH values. The inset shows the dependence of coercivity ( $H_C$ ) of the samples on pH.

The  $H_C$  moves up from 22.9 Oe to 48.0 Oe with the pH value increasing from 5.0 to 7.0, then the  $H_C$  slightly reduces to 42.4 Oe as the pH value increases to 8.0. The evolution of  $H_C$  with pH is

related to the microstructure of the samples. As was shown in Fig. 1, when the pH is increased from 5.0 to 7.0, the particles in the films become smaller. The reduction of particle size may bring about the increase of  $H_C$  according to magnetic domain theory [29, 30]. When the pH value is higher than 7.0, the particle size is further decreased (Fig. 1d), the  $H_C$  of the sample decreases due to thermal effect [31, 32].

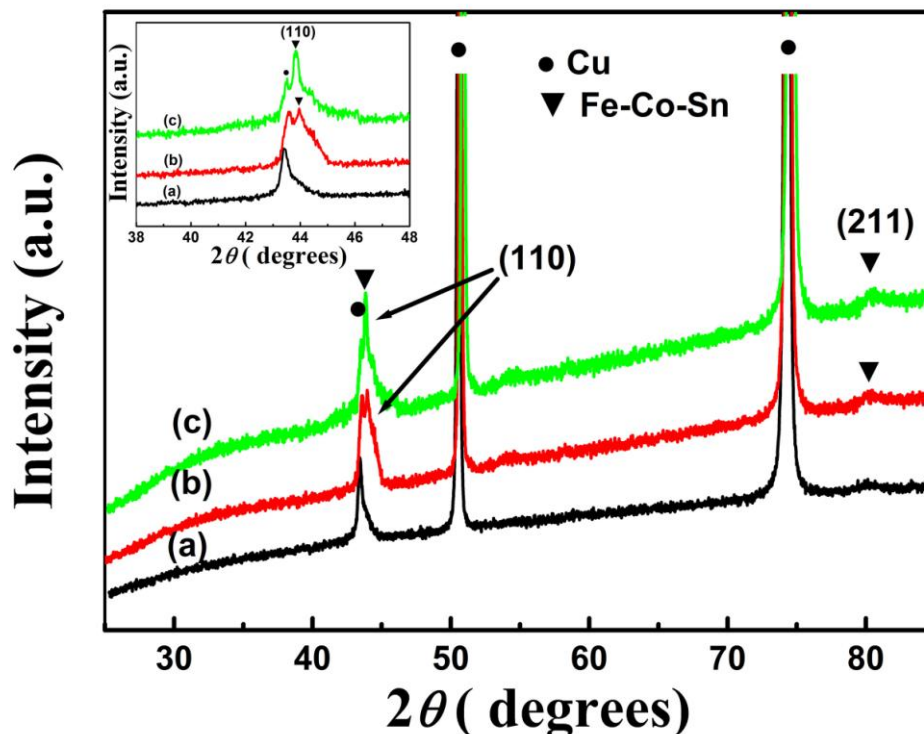
### 3.2. Effects of deposition time

Fig. 5 shows the surface morphologies of the samples deposited at 5 min, 15 min and 25 min when the electrolyte pH is 7.0. When the deposition time is 5 min (Fig. 5a), the film is composed of small particles and raised particle aggregations (inset in Fig. 5a). When the deposition time is 15 min (Fig. 5b), the film is full of fine particles with the size of about 20-30 nm. As the deposition time is extended to 25 min (Fig. 5c), the film is finely crystalline and compact. It can be seen that with the increasing of deposition time, the film surface becomes uniform. The film thickness of the samples measured by taking vertical cross section SEM is about 2  $\mu\text{m}$ , 7  $\mu\text{m}$  and 9  $\mu\text{m}$  for the samples deposited at 5 min, 15 min and 25 min, respectively. It can be seen that the film thickness tends to increase with the deposition time.



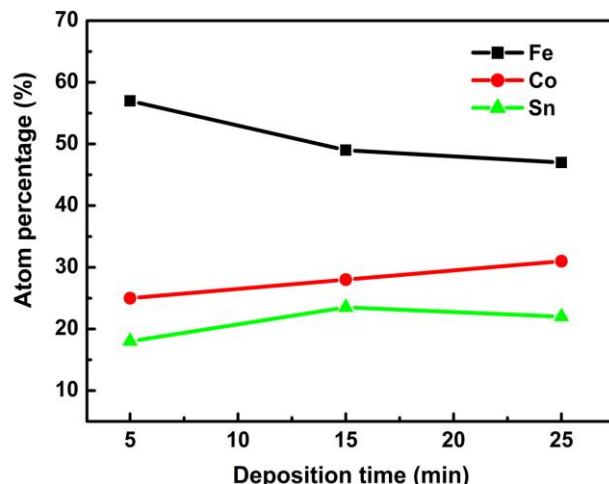
**Figure 5.** SEM images of the samples deposited at different deposition times. (a) 10 min; (b) 15 min; (c) 25 min.

Fig. 6 shows the XRD patterns of the samples deposited at 5 min, 15 min and 25 min when the pH=7.0. When the deposition time is 5 min (Fig. 6a), only the diffraction peaks of Cu substrate are observed. During this period, there are not enough nuclei on the substrate, such effect may explain the absence of Fe-Co-Sn diffraction peaks as shown in Fig. 6a [33]. For the samples deposited at 15 min and 25 min (Fig. 6b-c and inset in Fig. 6), besides the peaks from the Cu substrate, the diffraction peaks at about  $2\theta = 44.0^\circ$  and  $2\theta = 81.0^\circ$  are present which correspond to the (110) and (211) characteristic reflections of bcc structure.



**Figure 6.** XRD patterns of the samples deposited at different deposition times. (a) 10 min; (b) 15 min; (c) 25 min. The inset shows the magnified (110) diffraction peaks of the XRD patterns.

The dependences of Fe, Co and Sn content in the samples on deposition time are shown in Fig. 7. It can be seen that as the deposition time is longer than 5 min, the content of Fe slightly decreases and the content of Sn slightly increases. When the deposition time is 5 min, Fe is preferentially deposited compared to Sn, so the content of Fe is high. After a long time deposition (15 min and 25 min), the consumption of  $\text{Fe}^{2+}$  near the cathode surface is larger than that of  $\text{Sn}^{2+}$ , however  $\text{Fe}^{2+}$  can't be supplied in time, so the content of Fe in the deposit slightly decreases. Accordingly, the content of Sn in the deposit increases [34].



**Figure 7.** The dependences of Fe, Co and Sn content in the samples on deposition time.

Fig. 8 shows the hysteresis loops of the samples deposited at different times. The inset in Fig. 8 displays the dependence of  $H_C$  on deposition time. With the extension of the deposition time, the  $H_C$  has a tendency to decrease.  $H_C$  is frequently reported to decrease when the film thickness increases [35, 36]. According to the Neel’s relation, with the increase of the film thickness, the  $H_C$  decreases [37]. In our samples, the film thickness increases with the deposition time, therefore, the  $H_C$  decreases with the increasing deposition time.

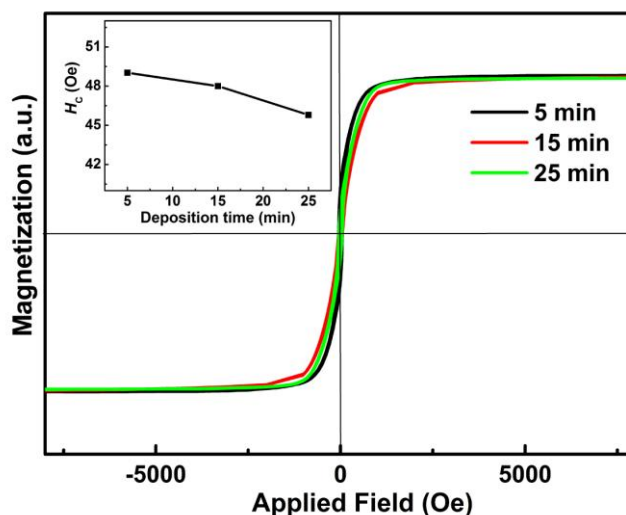


**Figure 8.** Hysteresis loops of the samples deposited at different deposition times. The inset shows the dependence of  $H_C$  of the samples on deposition time.

### 3.3. Characterization of $Fe_2CoSn$ Heusler alloy

According to the EDS results in Fig. 7, for the samples deposited at pH=7.0 with the deposition time of 15 min, the composition ratio of Fe:Co:Sn is about 2.0: 1.1:1.0, which is within experimental

error of the nominal 2: 1: 1 composition of  $\text{Fe}_2\text{CoSn}$ . Hence, the sample may be referred to as  $\text{Fe}_2\text{CoSn}$  Heusler alloy.  $\text{Fe}_2\text{YZ}$  Heusler compounds exhibit various types of structure depending on site disorders. If Fe atoms occupy the Wyckoff position 8c (1/4, 1/4, 1/4), Y and Z atoms are located at 4a (0, 0, 0) and 4b (1/2, 1/2, 1/2), respectively, the  $\text{Fe}_2\text{YZ}$  Heusler alloy will show the cubic  $L2_1$  ordered structure, If all atomic sites are equivalent, the  $\text{Fe}_2\text{YZ}$  Heusler alloy will show an A2-type disorder [body-centered cubic (*bcc*) lattice]. If Y and Z atoms randomly occupying the 4a and 4b positions, the  $\text{Fe}_2\text{YZ}$  Heusler alloy will show a B2 ordered structure (simple cubic lattice) [38]. According to the results of X-ray diffraction analysis (Fig. 6b), the sample prepared at pH = 7.0 using the deposition time of 15 min has *bcc* structure. Our XRD and EDS results show that A2-type cubic  $\text{Fe}_2\text{CoSn}$  Heusler alloy can be obtained using electrodeposition method when the pH value is 7.0 and the deposition time is 15 min.

In order to study the composition homogeneity of our  $\text{Fe}_2\text{CoSn}$  sample, EDS elemental mappings of the  $\text{Fe}_2\text{CoSn}$  film were performed. Fe, Co and Sn EDS mappings are shown in Fig. 9 which illustrate a homogeneous distribution of Fe, Co and Sn in the  $\text{Fe}_2\text{CoSn}$  sample.

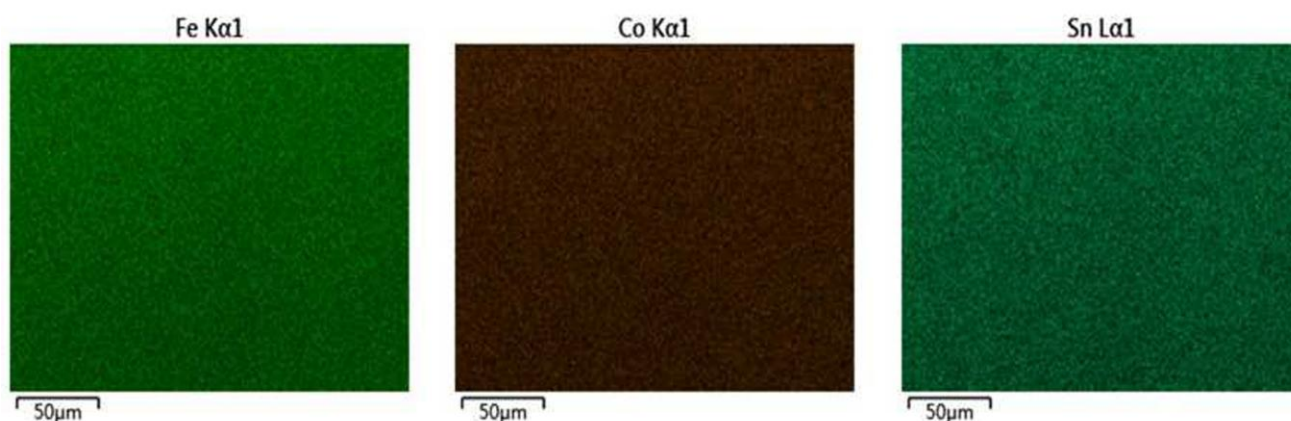


**Figure 9.** EDS elemental mappings of Fe, Co and Sn elements in the  $\text{Fe}_2\text{CoSn}$  film.

According to the magnetic measurement results (Fig. 8), the  $M_S$  of  $\text{Fe}_2\text{CoSn}$  sample is roughly estimated to be in the range of  $1300 \text{ emu/cm}^3$ . Accordingly, the magnetic moment per formula unit is calculated to be  $3.5 \mu_B$ . The value of magnetic moment is smaller than the theoretically predicted value of  $\text{Fe}_2\text{CoSn}$  Heusler alloy [17] and close to the  $\text{Fe}_2\text{CoGa}$  Heusler nanoparticles with the particle size of 20 nm which have a magnetic moment of  $3.59 \mu_B$  [39]. It is known from Fig. 8 that the  $H_C$  of  $\text{Fe}_2\text{CoSn}$  sample is 48 Oe at room temperature. The  $H_C$  of our  $\text{Fe}_2\text{CoSn}$  sample is comparable with the  $\text{Co}_{30}\text{Fe}_{70}$  nanoparticles with the particle size of 8 nm prepared by a chemical reduction method [40]. Compared with previous reports about the  $\text{Fe}_2$ -based Heusler alloy, such as  $\text{Fe}_2\text{MnGa}$  prepared by arc melting which have a  $H_C$  of about 60 Oe at room temperature [4], the value of  $H_C$  of our  $\text{Fe}_2\text{CoSn}$  sample is smaller.

#### 4. CONCLUSIONS

Our work demonstrated that Fe<sub>2</sub>CoSn Heusler alloy can be prepared by a cost-effective electrodeposition method. A contribution to the knowledge of electrolyte pH and deposition time dependence of surface morphology, structure, chemical composition, and magnetic properties of the electrodeposited films is reported. The relations between the microstructure and magnetic properties of the samples are given. The stoichiometric Fe<sub>2</sub>CoSn Heusler alloy with A2-type cubic structure was obtained by using the pH of 7.0 and deposition time of 15 min. The SEM image showed that the obtained Fe<sub>2</sub>CoSn alloy film is composed of many small particles with the size of about 20-30 nm. EDS mappings revealed the homogeneous distribution of Fe, Co and Sn element in the Fe<sub>2</sub>CoSn film. The magnetic moment of the Fe<sub>2</sub>CoSn alloy film is estimated to be 3.5  $\mu_B$  and the  $H_C$  is 48 Oe at room temperature.

#### ACKNOWLEDGEMENTS

The work was supported by the Natural Science Foundation of China (51201082), the National Training Program of Innovation and Entrepreneurship for Undergraduates (201510730067) and the Open Project of Key Laboratory for Magnetism and Magnetic Materials of the Ministry of Education, Lanzhou University (LZUMMM2015007).

#### References

1. T. Graf, C. Felser, and S. S. P. Parkin, *Prog. Solid State Chem.* 39 (2011) 1.
2. W. Zhu, E. K. Liu, C. Z. Zhang, Y. B. Qin, H. Z. Luo, W. H. Wang, Z. W. Du, J. Q. Li, and G. H. Wu, *Acta Phys. Sin.* 61 (2011) 027502.
3. A. Ayuela, J. Enkovaara, K. Ullakko, and R. M. Nieminen, *J. Phys.: Condens. Matter* 11 (1999) 2017.
4. T. Gasi, A. K. Nayak, M. Nicklas, and C. Felser, *J. Appl. Phys.* 113 (2013) 17E301.
5. M. Zhang, E. Brück, F. R. de Boer, and G. Wu, *J. Magn. Magn. Mater.* 283 (2004) 409.
6. T. Gasi, V. Ksenofontov, J. Kiss, S. Chadov, A. K. Nayak, M. Nicklas, J. Winterlik, M. Schwall, P. Klaer, P. Adler, and C. Felser, *Phys. Rev. B* 87 (2013) 064411.
7. A. Matsushita, T. Naka, Y. Takano, T. Takeuchi, T. Shishido, and Y. Yamada, *Phys. Rev. B* 65 (2002) 075204.
8. M. Nakabayashi, K. Fukuda, H. Kitagawa, Y. Yamada, S. Kubo, and A. Matsushita, *Physica B* 329-333 (2003) 1134.
9. Z. Ren, S. T. Li, and H. Z. Luo, *Physica B* 405 (2010) 2840.
10. T. Omori, K. Watanabe, R. Y. Umetsu, R. Kainuma, and K. Ishida, *Appl. Phys. Lett.* 95 (2009) 082508.
11. Y. Maeda, K. Narumi, S. Sakai, Y. Terai, K. Hamaya, T. Sadoh, and M. Miyao, *Thin Solid Films* 519 (2011) 8461.
12. D. Lin and X. Wang, *Surf. Coat. Technol.* 204 (2010) 3205.
13. C. Ni, H. Zhou, Z. Wang, Q. Yao, and L. Lu, *Int. J. Electrochem. Sci.* 9 (2014) 2397.
14. L. Jiang, Z. Jin, Y. Sun, P. Wu, Q. Peng, G. Wei, and H. Ge, *Int. J. Electrochem. Sci.* 9 (2014) 1715.
15. K. Leistner, S. Fähler, H. Schlörb, and L. Schultz, *Electrochem. Commun.* 8 (2006) 916.
16. J. Duan and X. Kou, *J. Electrochem. Soc.* 160 (2013) D471.
17. M. Gilleßen and R. Dronskowski, *J. Comput. Chem.* 30 (2009) 1290.

18. C. Qiang, J. Xu, S. Xiao, Y. Jiao, Z. Zhang, Y. Liu, L. Tian, and Z. Zhou, *Appl. Surf. Sci.* 257 (2010) 1371.
19. C. Han, Q. Liu, and D.G. Ivey, *Electrochim Acta* 53 (2008) 8332.
20. C. U. Chisholm, E. Sharif, E. Kuzmann, S. Stichleutner, Z. Homonnay, and A. Vertes, *Mater. Chem. Phys.* 120 (2010) 558.
21. M. Saito, N. Ishiwata, and K. Ohashi, *J. Electrochem. Soc.* 149 (2002) C642.
22. A. Vicenzo and P. L. Cavallotti, *Electrochim. Acta* 49 (2004) 4079.
23. L. Tian, J. Xu, and S. Xiao, *Vacuum* 86 (2011) 27.
24. T. R. Bergstresser and H. D. Merchant, *Defect structure morphology and properties of electrodeposits*, The Minerals, Metals & Materials Society, Eastlake (1995).
25. L. Zhu, S. Bai, H. Zhang, and Y. Ye, *Appl. Surf. Sci.* 265 (2013) 537.
26. M. Haerifar and M. Zandrahimi, *Appl. Surf. Sci.* 284 (2013) 126.
27. A. Brenner, *Electrodeposition of Alloys*, vols. 1 and 2, Academic press, New York and London (1963).
28. B. Robotin, A. Ispas, V. Coman, A. Bund, and P. Ilea, *Waste Manage.* 33 (2013) 2381.
29. B. D. Cullity, *Introduction to Magnetic Materials*, Addison-Wesley, Reading, MA (1972).
30. W. Gong, H. Li, Z. Zhao, and J. Chen, *J. Appl. Phys.* 69 (1991) 5119.
31. S. Gangopadhyay, G. C. Hadjipanayis, B. Dale, C. M. Sorensen, K. J. Klabunde, V. Papaefthymiou, and A. Kostikas, *Phys. Rev. B* 45 (1992) 9778.
32. C. Chen, O. Kitakami, and Y. Shimada, *J. Appl. Phys.* 84 (1998) 2184.
33. M. Gannouni, I. B. Assaker, and R. Chtourou, *Superlattices Microstruct.* 61 (2013) 22.
34. J. Zhang, D. Li, Y. Zhu, M. Chen, M. An, P. Yang, and P. Wang, *Electrochim. Acta* 151 (2015) 415.
35. J. H. Kefalas, *J. Appl. Phys.* 37 (1966) 1160.
36. D. Zhou, M. Zhou, M. Zhu, X. Yang, and M. Yue, *J. Appl. Phys.* 111 (2012) 07A319.
37. L. Néel, *J. Phys. Radium* 17 (1956) 250.
38. P. J. Webster, *Contemp. Phys.* 10 (1969) 559.
39. C. Wang, F. Casper, T. Gasi, V. Ksenofontov, B. Balke, G. H. Fecher, C. Felser, Y. K. Hwu, and J. J. Lee, *J. Phys. D: Appl. Phys.* 45 (2012) 295001.
40. C. W. Kim, Y. H. Kim, H. G. Cha, H. W. Kwon, and Y. S. Kang, *J. Phys. Chem. B* 110 (2006) 24418.